Proceedings of the Thirty-second (2022) International Ocean and Polar Engineering Conference **www.isope.org**
Shanghai, China, June 5–10, 2022

ISBN 978-1-880653-81-4; ISSN 1098-6189

Numerical Study of Wave-Structure Interaction with HOS-CFD Method

Yuan Zhuang[1], Jianhua Wang[1], Wenjun Zhou[2], Cong Liu[2], Decheng Wan[1]*
[1] State Key Laboratory of Ocean Engineering, School of Naval Architecture, Ocean and Civil Engineering, Shanghai Jiao Tong University, Shanghai, China
[2] Marine Design and Research Institute of China, Shanghai, China
[*] Corresponding Author

ABSTRACT

In the present work, a HOS-CFD coupled method is validated with wave-structure interaction. The HOS-CFD method is applied to simulate a fixed CALM buoy in regular waves with overset grids. Firstly, a periodic wave simulation is carried out to make a better parameter choice in HOS-CFD method combined with overset grids. Secondly, the forces and scattered waves around the CALM buoy are obtained through computations. The results are compared with experimental results to validated the coupled method. The results of the numerical method are compared with other numerical methods, including CFD methods and other potential-viscous methods. It is shown that the coupled method with overset technique is reliable in predicting wave-structure interactions. At last, a Q-criterion and liutex view of turbulence flow are considered both in overset grids and static grids, give the difference between these two mesh generations in HOS-CFD coupled method.

KEY WORDS: HOS; HOS-CFD coupled method; naoe-FOAM-SJTU solver; CALM buoy

INTRODUCTION

With the developing and exploiting marine resources into deep sea, the study of hostile environment and wave-structure interaction became essential. The floating platforms in deep sea may face freak waves which induce large movement. Traditional CFD method with dynamic mesh technique may have some weaknesses in solving this kind of problem, for example, source cost due to long-time simulation and mesh break due to large motion amplitude. Therefore, a new coupled method on studying wave and structure interaction is required. As we want to solve this kind of problem efficiently and accurately, the viscous effect around the body need to be included. Thus, the potential-viscous coupled method is adopted, including the overset grid method.

The coupling method of potential and viscous method can be divided into two categories, functional-decomposition coupling and domain-decomposition coupling (Li, 2018). The functional-decomposition coupling method considered solving the whole problem in the same computational domain, for example, Helmholtz velocity decomposing theorem (Morino, 1986) is a common functional-decomposition coupling method. Dommermuth (1998) applied this method into hydrodynamic problem, and he used this method to study the bow wave. Zhao et al(2016, 2017) applied Helmholtz velocity decomposing theorem into the open source software OpenFOAM, solving the flow around the SUBOFF and a cylinder. Another functional-decomposition coupling method is SWENSE (Spectral Wave Explicit Navier-Stokes Equations) (Ferrant, 2002, 2003). This method divided the computational variables into incident variables and radiation variables. The domain-decomposition coupling method combined potential computational domain and viscous computational domain together, just match the boundary condition of these two methods. The advantage of domain-decomposition method is the ability to achieve the two-way coupling easily. For example, Kim et al (2010) applied two-way coupling of BEM and VOF method to study the random waves. However, the two-way coupling method is still complex and cost time on the iterate solution. Therefore, many studies applied one-way coupling method, such as Lachaume et al (2003) and Biausser et al (2003, 2004). They combined BEM and VOF to solve the wave propagating on the slope. In general, the potential-viscous method applied BEM method as the potential method. However, Ducrozet et al (2014) mentioned that BEM method needs to be improved in efficiency.

In the present work, we combine our in-house CFD solver naoe-FOAM-SJTU with a pseudo-spectral method High-Order-Spectral method (HOS). HOS method is a pseudo-spectral method (Dommermuth, D.G. and Yue, D.K.P, 1987). It based on the partial difference equation on dynamic and kinematic free surface boundary condition. The potential on the surface are wrote in a perturbation series and expanded each order in a Taylor series. Thanks to the Fast Fourier Transform (FFT), the communication between discretization space and modal space is very fast. With the given initial variables, the unknown potential can be obtained. Therefore, HOS method can generate nonlinear wave in a fast and efficient way. The combination of CFD method and HOS have done in previous work (Zhuang et al, 2018, 2021), including freak wave with ship motion interaction (Zhuang et al, 2020) and combination with overset grids (Zhuang et al, 2020). The HOS-CFD coupled method with

overset grids have been validated with moving container ship (Zhuang et al, 2020). However, there still exits some discrepancies between numerical results and experimental results. In order to figure out the existence of discrepancies is caused by whether the overset grids or the combination method, in this paper, an empty grid and a fixed structure with overset grids are studied.

The combined solver is discussed in detail and validation is shown. A periodic stream function wave is generated by an open source HOS software named HOS-Ocean (Ducrozet, G. et al, 2016). A parametric study with empty overset grid is generated to figure out the parametric choice in this combined solver. A CALM buoy in the wave is also studied to validate the combined solver.

METHODOLOGY

CFD method

The CFD method uses our in-house solver naoe-FOAM-SJTU (Wang et al., 2019), which is based on the open source software OpenFOAM. The incompressible Navier-Stokes equations are adopted to calculate the flow field:

$$\nabla \cdot \mathbf{U} = 0 \tag{1}$$

$$\rho \frac{\partial \mathbf{U}}{\partial t} + \mathbf{U} \bullet \nabla (\mathbf{U} - \mathbf{U}_g) = -\nabla p_d - \mathbf{g} \bullet \mathbf{x} \nabla p + \mu \nabla^2 \mathbf{U} + \mathbf{f}_\sigma \tag{2}$$

where $\mathbf{U}$ is velocity field, $\mathbf{U}_g$ is velocity of grid nodes; $p_d = p - \rho \mathbf{g} \cdot \mathbf{x}$ is dynamic pressure; $\mathbf{x}$ is the horizontal direction which is based on the Cartesian coordinates; $\mathbf{f}_\sigma$ is the surface tension term in two phases model.

The solution of momentum and continuity equations is implemented by using the pressure-implicit spit operator (PISO) algorithm (Issa, R.I. 1986). The Volume of fluid (VOF) method is applied to capture the two-phase interface. The VOF transport equation is described below:

$$\frac{\partial \alpha}{\partial t} + \nabla \bullet [(\mathbf{U} - \mathbf{U}g)\alpha] = 0 \tag{3}$$

Where α is volume of fraction, indicating the relative proportion of fluid in each cell and its value is always between zero and one:

$$\begin{cases} \alpha = 0 & \text{air} \\ \alpha = 1 & \text{water} \\ 0 < \alpha < 1 & \text{interface} \end{cases} \tag{4}$$

High Order Spectral Method

The potential flow method is HOS (High Order Spectral Method) method. The formulation of HOS method is based on the free surface velocity potential. The surface potential can be defined as (Zakharov, 1968):

$$\phi^S(\boldsymbol{x}, t) = \phi(\boldsymbol{x}, \eta(\boldsymbol{x}, t), t) \tag{5}$$

According to the formulation of equation (5), the dynamic and kinematic boundary condition can be expressed as :

$$\eta_t + \nabla_x \phi^S \bullet \nabla_x \eta - (1 + \nabla_x \eta \bullet \nabla_x \eta)\phi_z(\boldsymbol{x}, \eta, t) = 0 \tag{6}$$

$$\phi_t^S + \eta + \frac{1}{2}\nabla_x \phi^S \bullet \nabla_x \phi^S - \frac{1}{2}(1 + \nabla_x \eta \bullet \nabla_x \eta)\phi_z^2(\boldsymbol{x}, \eta, t) = -Pa \tag{7}$$

where ϕ^S is the surface potential. With the known initial velocity potential and surface elevation, the unknown ϕ can be solved as:

$$\phi^S(\boldsymbol{x}, t) = \sum_{m=1}^{M} \sum_{k=0}^{M-m} \frac{\eta^k}{k!} \frac{\partial^k}{\partial z^k} \phi^{(m)}(\boldsymbol{x}, 0, t) \tag{8}$$

Expanding ϕ in a perturbation series and then further expand each order of ϕ evaluated on free surface in a Taylor series. With the help of Fast Fourier Transform (FFT), the information can be rapidly transported between mode space and physical space.

Combination with HOS and CFD

The combination between HOS and CFD chooses domain-decomposition coupling method. When wave interacts with structures, the viscous effect only exists around structures and can be ignored in far fields. Therefore, the domain-decomposition coupling method can be described as applying CFD method near the body while using potential theory far away from body.

The domain-decomposition coupling method is a simple procedure in dealing with the combination between HOS and CFD method, just considering match the boundary condition of these two methods. The first step is to interpolate the time step and wave field information in HOS grid. The HOS method requires less need for time steps and mesh size than that in CFD method. The interpolation method we used is based on a HOS wrapper program called Grid2Grid (Choi, 2017).

The second step is to build an interface in CFD domain to receive the wave field from HOS and propagate the wave information into viscous domain. The interface we applied is based on a relaxation scheme(Jacobsen, N.G. et al, 2012):

$$\phi = \alpha_R \phi_{computed} + (1 - \alpha_R)\phi_{target} \tag{9}$$

where ϕ_{target} is the parameters such as velocity potential and wave elevation in HOS, $\phi_{computed}$ is the original parameters in CFD, ϕ is the final parameters in wave propagation, α_R is weighting factor. The value of weighting factor is from 0 to 1. There are three kinds of weighting factors, we applied power weight in this paper:

$$\omega_R = 1 - \frac{\exp \sigma^p - 1}{\exp 1 - 1} \tag{10}$$

The default value of power exponent p is 3.5. σ is the local coordinate value in the relaxation area, which is determined according to the shape of the relaxation area.

The variation of the weighting factor is shown in Fig. 1. In the meantime, the implementation of relaxation zone can avoid wave reflection, therefore it can be a wave damping function as well.

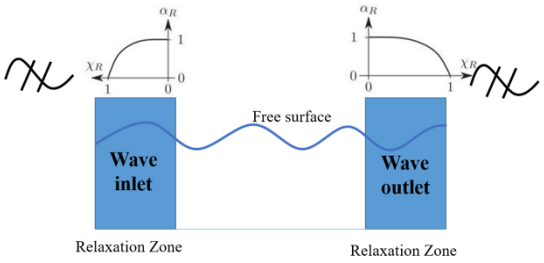

Fig. 1 The relaxation zone in inlet and outlet

Fig.2 illustrates the calculation process in combined solver, the whole simulation process can be described as below:

(a) Generating the wave field applying HOS method and saving the results file.
(b) Manually find the needed wave field, including the simulation time and domain size.
(c) Matching the simulation time in HOS method and that in CFD method.
(d) Applying relaxation scheme to receive wave information from the HOS method, and propagate wave field into viscous zone.
(e) Solving N-S equation, before reach the final time spot, return to (c).

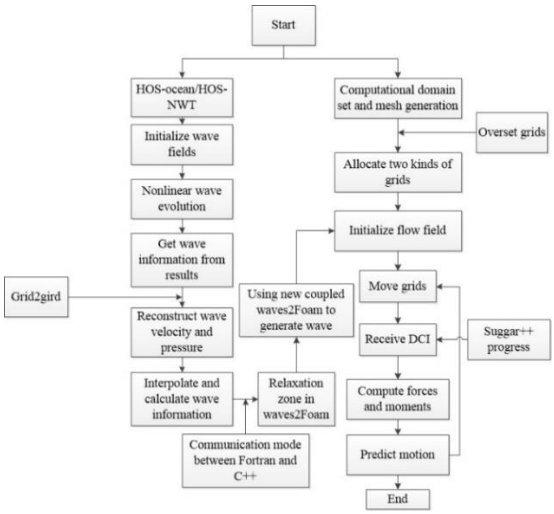

Fig. 2 The calculation process of the combined solver

The whole simulation process is much similar with that without overset grids, despite the process in solving the interpolation between two grids. Before solving wave-structure interaction, an empty overset grid is carried out to figure out the accuracy of overset grid scheme in the combined solver.

In order to chase for a better parameter choice and test the steady of the current combination method, a periodic wave simulation is carried out. The wave condition is chosen as fully nonlinear waves (Stream Function wave), and the wave propagates with periodic boundary condition. The wave is 0.8082 meters long, with period of 0.7018 seconds. The wave amplitude is 0.0288 meters. The dissipation in interacted mesh scheme are discussed in this simulation. To figure out whether wave propagation will keep still in overset grids, an overset grid without body are displaced with an oscillate movement along the free surface.

Fig.3 shows the movement of the overset grids in periodic boundary condition. The motion of the grid is almost like oscillation. It both have translation and rotation as well. The motion of translation is x=0.5cos(4t), while the motion of rotation is w=cos4t. The length of computational domain is also ten times of wave length, the same with normal mesh case. The setup of six cases are shown in Table 1.

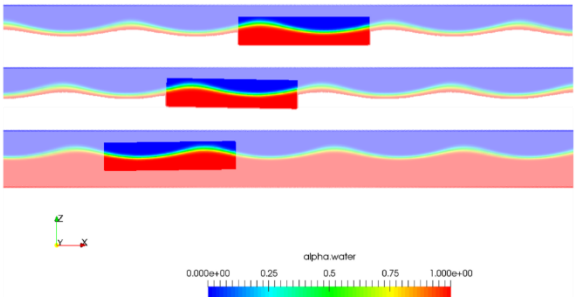

Fig. 3 The setup of simulation of overset grids case

Table 1 Parameters of noninear regular wave and irregular wave

Name	$\lambda/\Delta x$	$H/\Delta z$	t/T	Time integration
Euler	100	20	800	Euler
CN0.9	100	20	800	Crank-Nicolson, 0.9
CN0.95	100	20	1400	Crank-Nicolson, 0.95
mesh-10	50	10	400	Crank-Nicolson, 0.95
mesh-20	100	20	1400	Crank-Nicolson, 0.95
mesh-40	200	40	1400	Crank-Nicolson, 0.95

Three different time integration and three different mesh generation are displaced. The Crank Nicolson scheme (Giles and Carter, 2005) with different weighting factors are different. When the value of weighting factor chooses 0, the scheme is implicit Euler integration scheme; when the value of weighting factor chooses 1, the scheme is explicit Crank Nicolson scheme. Fig.4(a) shows the first harmonic wave in three different time integrations. It can be seen that wave dissipated more quickly in Euler while more slowly in C-N scheme with 0.95 weighting factor.

As for the overset grid cases, the instability increases between the fine background and hull meshes. In order to ensure the stability of the cases, the time step is adjusted. It can be seen that the time integration scheme is more accurate, the stability is worse. Therefore, a smaller time step is needed to stabilize the fine mesh case; Similarly, the time step should be increased when the cell number of the mesh is large.

Fig.4(b) provides the first harmonic wave elevation in 40 periods with different mesh generation. It can be observed that mesh-20 and mesh-40 show little difference in wave elevation.

These six cases give a probable parameter choice of overset grids in combination solver. The numerical dissipation increases due to the long-time simulation and coarse mesh generation, and the overset grids rarely influence the wave propagation.

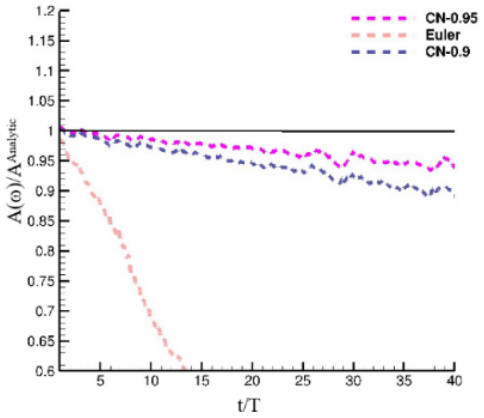

(a) different time integration schemes

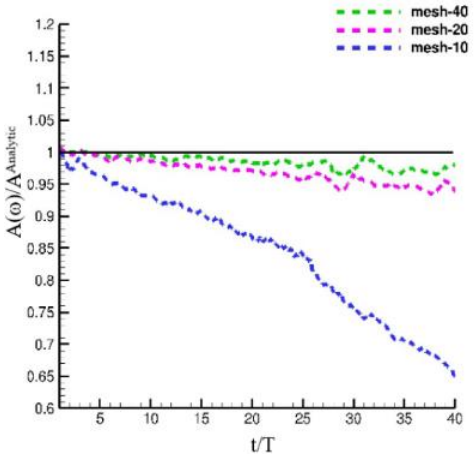

(b) different mesh generations

Fig. 4 First harmonic wave elevation in different cases

NUMERICAL SIMULATION

Numerical Setup

The numerical model was chosen to be a fixed body in the numerical tank. The test case is based on an experiment carried out in the ocean wave basin of Ecole Centrale de Nantes (50m long, 30m wide and 5m deep). The experiments are focused on the interaction between regular wave and irregular wave with a fixed CALM buoy. The buoy has a truncated cylinder form with a thin skirt near the bottom to provide additional damping forces through vortex shedding. The details of the parameters of the CALM buoy can be found in (Li et al, 2018). Both regular wave condition and irregular wave condition are considered, and the test conditions are illustrated in Table 2.

Table 2 Parameters of nonlinear regular wave and irregular wave

Parameters	Value
Period（T）	1.8 s
Wave height（H）	0.16 m
Wave length（λ）	5.05 m
Wave steepness（ka）	0.10

Fig. 5 shows the CALM buoy in the experiment. In order to validate the new coupled method, three wave probes are added around the CALM buoy in numerical simulation, which is the same setup with that in the experiment. The three probes are displaced 1.15m away from the center of the buoy and formed 0 ˚. 90 ˚and 180 ˚with the direction of incident wave.

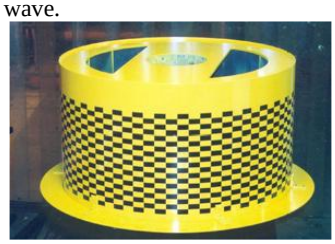

Fig.5 CALM buoy in experiment setup

The origin of coordinate is set in the center of the buoy. The mesh generation chooses half of the buoy for it is center-symmetry. The selected CFD computational domain is described as -10.1m<x<15.15m, 0<y<15.15m, -5.25m<z<2.25m, which refers to the work of Li et al(2020). In their work, the results show that when there are 80 grids in one wave length, the forces on the buoy is the closest with that in experiment.

The mesh distribution in overset grids is shown in figure 6, with the computational domain of buoy is set as -1.25m<x<1.25m, 0<y<1.6m, -0.8m<z<0.8m. The background mesh and body mesh are both generated by *snappyHexMesh*, an mesh generation tool provided by OpenFOAM. In order to capture the wave around the body and the thin skirt, mesh around the free surface and buoy are refined.

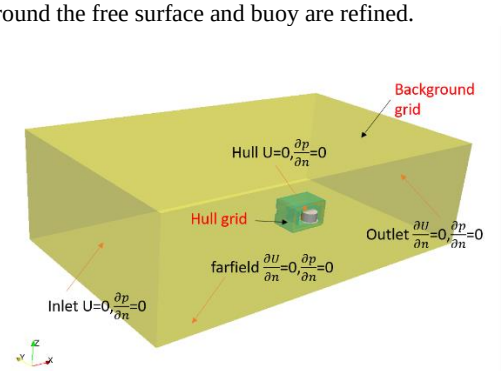

(a) Overset mesh of computational domain in CFD zone

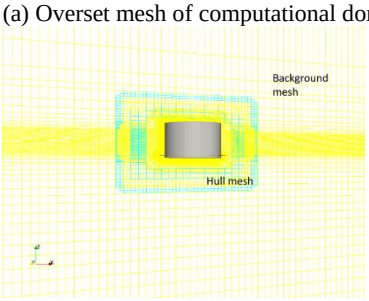

(b) Overset mesh generation around the CALM buoy

Fig. 6 The setup of computational domain

In order to validate the accuracy of the new coupled method, a mesh convergence study is carried out. From Cell A to Cell C, the grid number in background mesh increases from 40 grids per wave length to 80 per wave length in x direction. They all have 20 grids per wave length in y direction and 16 grids per wave height. The history of horizontal force on buoy is shown in Fig.7. It can be observed that when the grid number chooses to be 40 per wave length in x direction, the results is converged. When the grids number increase to 80 per wave length, the value of the horizontal force doesn't change. Therefore, the mesh generation of Cell B is chosen in present study.

Table 3 Mesh generation

Name	Grids number	Background	Body	Total
Cell A	40L	0.86M	0.36M	1.22M
Cell B	40L	0.86M	1.38M	2.24M
Cell C	80L	1.08M	1.94M	3.02M

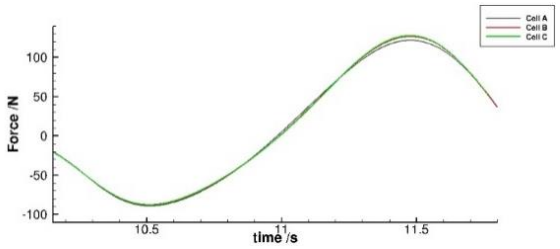

Fig. 7 The time history of horizontal force in different mesh generations

Forces and Scattering Waves

The time history of horizontal and vertical forces on buoy are shown in Fig. 8 (a) and Fig.9 (a). The wave is generated by the open source software HOS-Ocean. In order to compare the numerical results among experimental results and those in other numerical methods, a sliding window Fourier transform is processed with forces and scattering waves. The first order harmonic component of forces with simulation time is analyzed within 7 periods, shown in Fig.8 (b) and Fig.9 (b). The first crest value of the harmonic amplitude represents the time when the wave encounters with the buoy. The lowest point after the maximum value of the harmonic amplitude represents numerical dissipation. With the increase of the simulation time, the amplitude of the incident wave from inlet boundary begins to dissipate. After reaching the first decrease point, the simulation begins to keep stable. According to the Fig.8 (b) and Fig.9 (b), it can be overserved that using present method, the horizontal force remains stable after 3 periods while vertical force uses 4 periods. With the existence of the thin skirt, the vertical force is less easily to reach stable.

In order to do the comparison with experimental data, the forces are non-dimensionalized as:

$$F(x)=\frac{F_h}{A_m k\rho g V} \tag{11}$$

$$F(z)=\frac{F_v}{A_m k\rho g V} \tag{12}$$

where F_h and F_v is horizontal force and vertical force on CALM buoy, respectively. A_m is the incident wave amplitude, k is the wave number and V is the displacement volume.

Table 4 lists the results of forces on CALM buoy, including experimental methods, other three numerical methods and present methods. The values include first order and seconded order harmonic amplitudes. foamStar (Li et al, 2020) also used relaxation zone to generate wave fields. They applied implicit relaxation scheme. The results named foamStar-SWENSE applied SWENSE method, which is Spectral Wave Explicit Navier-Stokes Equations (Ferrant et al, 2003; Vukčević et al., 2016; Li et al., 2018, 2020). ISIS-CFD(Li et al, 2019) applied IWG method (Larsen and Dancy，1983；Lin and Liu, 1999；Choi and Yoon, 2009), which is Boussinesq equation added source term into N-S equation.

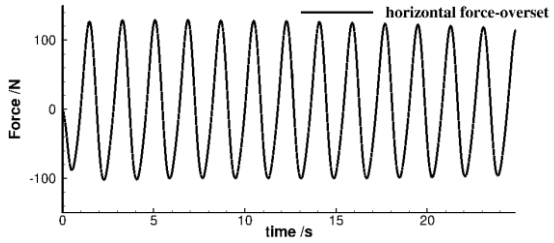

(a) Time history of horizontal force

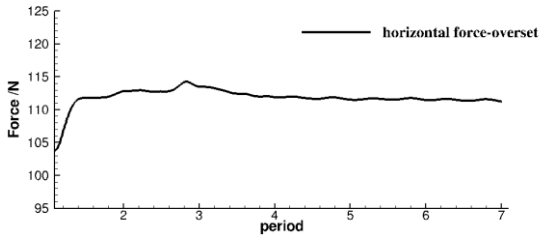

(b) The first order harmonic amplitude of horizontal force

Fig. 8 Force on buoy in horizontal direction

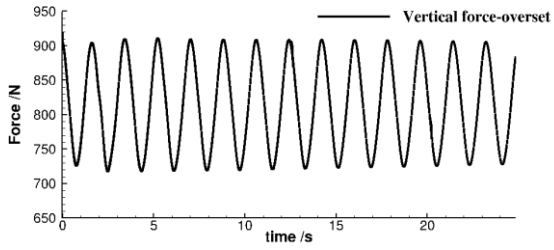

(a) Time history of vertical force

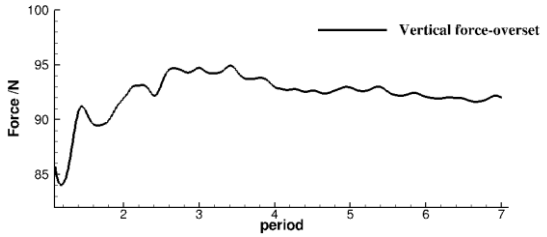

(b) The first order harmonic amplitude of vertical force

Fig. 9 Force on buoy in vertical direction

Table 4 Comparison among the forces of present method, experiment and other numerical methods

Data source		$F(x)^1$	$F(x)^2$	$F(z)^1$	$F(z)^2$
Experiment (Rousset, Ferrant, 2005)	80L	1.390	0.170	1.180	0.015
foamStar (Li. et al., 2020)	80L	1.359	0.168	1.098	0.010
foamStar-SWENSE(Li et al., 2020)	80L	1.387	0.186	1.149	0.012
ISIS-CFD (Li et al., 2019)	80L	1.378	0.173	1.141	0.014
naoe-FOAM-SJTU (Overset mesh)	40L	1.37	0.168	1.142	0.011
naoe-FOAM-SJTU (Static mesh)	80L	1.362	0.170	1.149	0.012

It can be seen that the value of first order components are larger than that

in second order components, which means the first order components represent the dominant physical problems. The value of first order components in numerical methods are all smaller than that in experimental results, our present method shows 1.4% error in horizontal force and 3.2% error in vertical force with experimental results.

In present method, a static mesh generation also considered and the results are listed in the table. With larger mesh grids in x direction as well as z direction, static mesh case shows better result in first order vertical force but worse result in first order horizontal force.

Fig. 10 shows the time history of three wave probes, which are the scattering waves around the CALM buoy. The trend of the harmonic amplitude curves of wave elevation is almost the same with that of forces. The first crest point represents the time when the first wave crest encounter with the wave probe, and the lowest point after the maximum value of the harmonic amplitude represents the numerical dissipation when the waves pass the buoy. The harmonic amplitude in the third wave probe shows two crest points, which implies the apparent reflection wave around the buoy in that position.

The scattering waves are non-dimensionalized as:

$$\eta = \frac{\eta_c}{A_m} \tag{12}$$

where η_c is the wave amplitude around the buoy.

Table.5 lists the results of wave elevation around CALM buoy, including first order and seconded order harmonic amplitudes of wave elevations. The value of all three wave elevations are larger than the amplitude of incident wave, and the maximum value locates on the first wave probe. The most obvious influence of buoy on the scattering wave field is near the incident wave direction. The error between first order harmonic amplitudes of wave elevation at wave probe 1, 2 and 3 with experimental results is about 8% and 1%, respectively.

Although the first order harmonic amplitudes of wave elevation are in good agreement with the experimental results, the discrepancy cannot be ignored. This may due to the measurement in overset grids but not the numerical error.

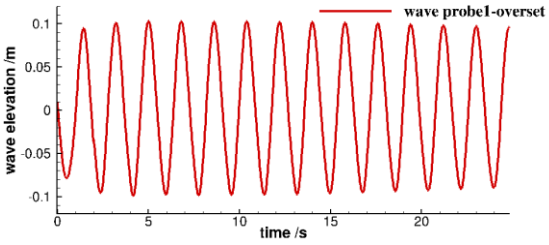

(a) Time history of wave elevation in wave probe 1

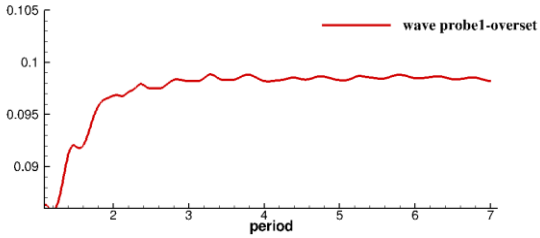

(b) The 1st harmonic amplitude of wave elevation in wave probe 1

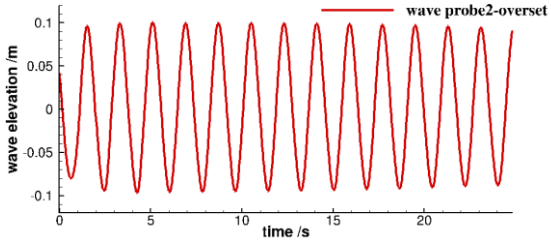

(c) Time history of wave elevation in wave probe 2

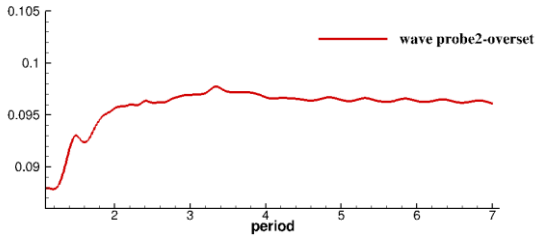

(d) The 1st harmonic amplitude of wave elevation in wave probe 2

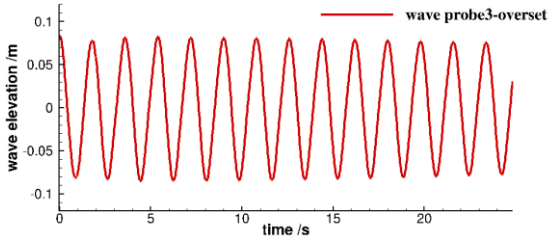

(e) Time history of wave elevation in wave probe 3

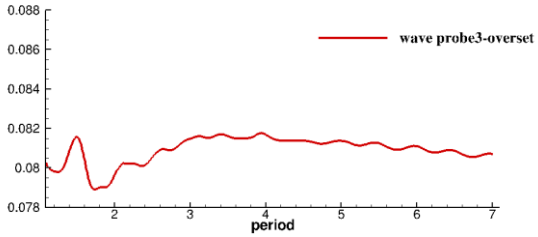

(f) The 1st harmonic amplitude of wave elevation in wave probe 3

Fig. 10 The wave elevation around the CALM buoy

Table 5 Comparison among the forces of present method, experiment and other numerical methods

Data source	η_1^1	η_1^2	η_2^1	η_2^2	η_3^1	η_3^2
Experiment (Rousset., Ferrant,2005)	1.220	0.065	1.210	0.040	1.040	0.035
foamStar (Li. et al., 2020)	1.195	0.06	1.18	0.036	1.002	0.045
foamStar-SWENSE (Li et al., 2020）	1.213	0.063	1.197	0.039	1.037	0.040
ISIS-CFD (Li et al., 2019）	1.224	0.064	1.208	0.040	1.041	0.050
naoe-FOAM (overset mesh)	1.12	0.06	1.11	0.05	1.033	0.06
naoe-FOAM (static mesh)	1.2	0.06	1.193	0.035	1.025	0.050

Wave field and Vortex

Fig. 11 shows the wave field around the CALM buoy both in overset grid and static grid. The time spot is chosen when wave crest passes through the buoy. For the value of wave steepness is 0.1, an obvious radiation wave around the buoy is observed. It can be seen that the wave field around buoy in two kinds of grids show little differences, therefore, the views of vortex are carried out next.

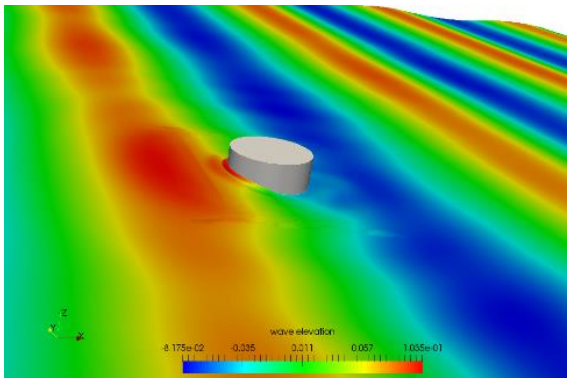

(a) overset grid

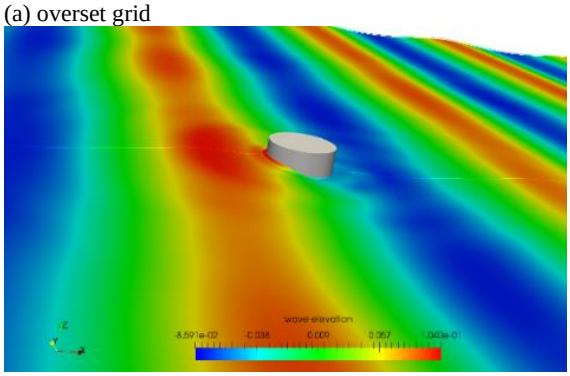

(b) static mesh

Fig.11 Flow field around CLAM buoy

Fig.12 illustrates vortex around the buoy in two kinds of grids, and countered by pressure. The view of the turbulent flow adopted Q criterion, which is based on the invariant quantity Q. The Q-criterion is formulated as:

$$Q = \frac{1}{2}[\|sym(\nabla u)\|_F^2 + \|skew(\nabla u)\|_F^2] \quad (13)$$

where sym and skew are the operators to obtain the symmetric and skew parts of the velocity gradient tensor, while $\| \|_F^2$ is a 2-norm value operator. The vortex in overset grid shows difference with that in static mesh grid, especially the vortex which appears under the free surface. The vortex near under the free surface is continuous in static mesh but fractured in overset grid.

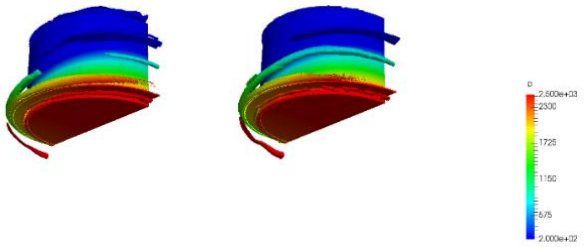

(a) overset grid (b) static mesh

Fig. 12 Vortex around the buoy in Q-criterion

Liu et al (2019) pointed out that the Q-criterion has only iso-surface can be displaced, without rotational axis or vortex direction obtained. Therefore, they developed a new vortex definition named 'Liutex', which defined the rotation part of the vorticity and can clearly represent the direction and magnitude of the rotational motion (2018).

Fig. 13 illustrates the vortex of two different grids in Liutex. It can be seen that the lacked vortex under free surface in overset grid is shown under Liutex estimation.

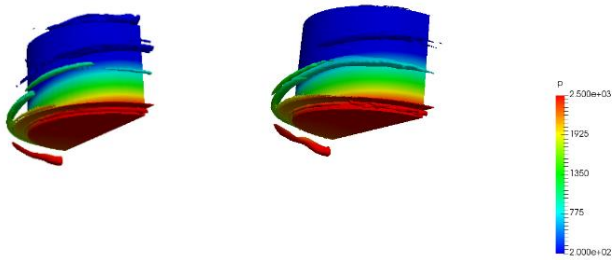

(a) overset grid (b) static mesh

Fig. 13 Vortex around the buoy in 'Liutex'

CONCLUSIONS

The potential-viscous method based on HOS-CFD approach is applied in the present research for wave-structure interaction. An empty overset grid is simulated to do the parametric study. The first order harmonic amplitude illustrates that the wave can be propagated smoothly through overset grid. Then a CALM buoy in overset grid is simulated and compared with three different numerical methods. The results of our method with overset grid agree fairly well with that in experiment, the discrepancies are due to numerical dissipation, which are acceptable.

The results in static mesh and overset mesh are also compared. The grid convergence study shows that when there is 40 grids per wave length in x direction with overset grid, the simulation is converged. Comparing with static mesh grids with 80 grids per wave length, the overset grids show similar numerical results.

This paper gives a HOS-CFD coupled method with overset grid on simulating a fixed CALM buoy in waves. The coupled method with overset technique is validated in this paper. Although the method with a moving container was simulated in previous work, the validation is done in this paper to reduce the numerical error due to body motion. The result shows that there is not much difference between these two methods.

ACKNOWLEDGEMENTS

This work is supported by the National Key Research and Development Program of China (2019YFB1704205), the National Natural Science Foundation of China (51809169), to which the authors are most grateful. This work is also thankful to Dr. Benjamin Bouscasse and Dr. Zhaobin Li in LHHEA, Ecole Centrale de Nante, which gave the author technique support and advices.

REFERENCES

Biausser B, Grilli S T, Fraunié P. (2003). "Numerical simulations of three-dimensional wave breaking by coupling of a VOF method anda boundary element method." *In Proceedings of The Thirteenth*

International Offshore and Polar Engineering Conference. International Society of Offshore and Polar Engineers, 333-339.

Biausser B, Fraunié P, Grilli S T, Marcer, R. (2004). "Numerical analysis of the internal kinematics and dynamics of 3-D breaking waves on slopes." *International Journal of Offshore and Polar Engineering*, 14(04), 247-256.

Choi, Y. M., Gouin, M., Ducrozet, G., Benjamin, B., Pierre, F. (2017). "Grid2Grid: HOS Wrapper Program for CFD solvers," *arXiv preprint arXiv:*1801.00026.

Dommermuth, D. G., Yue, D. K. P. (1987). "A high-order spectral method for the study of nonlinear gravity waves," *Journal of Fluid Mechanics*, 184: 267-288.

Dommermuth D, Innis G, Luth T, Novikov E, Schlageter E, Talcott J. (1998). "Numerical simulation of bow waves." *In Proceedings of the 22nd Symposium on Naval Hydrodynamics*, Washington, DC, U.S.A., 508 – 521.

Ducrozet G, Engsig-Karup A P, Bingham H B, Ferrant, P. (2014). "A non-linear wave decomposition model for efficient wave–structure interaction. Part A: Formulation, validations and analysis."*Journal of Computational Physics*, 257: 863-883.

Ducrozet, G., Bonnefoy, F., Le Touzé, D., Ferrant, P. (2016). "HOS-ocean: Open-source solver for nonlinear waves in open ocean based on High-Order Spectral method," *Computer Physics Communications*, 203: 245-254.

Ferrant P, Gentaz L, Le Touz´e D. (2002). "A new RANSE/Potential approach for water wave diffraction." *In Proceedings of Numerical Towing Tank Symposium*.

Ferrant P, Gentaz L, Alessandrini B, Le Touz´e D. (2003). "A potential/RANSE approach for regular water wave diffraction about 2-D structures." *Ship Technology Research*, 50(4): 165-171.

Issa, R. I. (1986). "Solution of the implicitly discretized fluid flow equations by operator-splitting," *Journal of computational physics*, 62(1), 40-65.

Jacobsen, N. G., Fuhrman, D. R., Fredsøe, J. (2012) "A wave generation toolbox for the open - source CFD library: OpenFoam®," *International Journal for numerical methods in fluids*, 70(9): 1073-1088.

Kim S H, Yamashiro M, Yoshida A. (2010). "A simple two-way coupling method of BEM and VOF model for random wave calculations. " *Coastal Engineering*, 57(11-12): 1018-1028.

Lachaume C, Biausser B, Fraunié P, Grilli, S. T., & Guignard, S. (2003). "Modeling of breaking and post-breaking waves on slopes by coupling of BEM and VOF methods." *In Proceedings of The Thirteenth International Offshore and Polar Engineering Conference*. International Society of Offshore and Polar Engineers, 353-359.

Li Z B. (2018). "Two-phase spectral wave explicit Navier-Stokes equations method for wave-structure interactions." Nantes: Ecole Centrale de Nantes.

Li, Z., B. Bouscasse, L. Gentaz, G. Ducrozet, and P. Ferrant. (2018). "Progress in coupling potential wave models and two-phase solvers with the SWENSE methodology", *In ASME 37th International Conference on Ocean, Offshore and Arctic Engineering*.

Liu, C., Gao, Y. S., Dong, X. R., Wang, Y. Q., Liu, J. M., Zhang, Y. N., ... & Gui, N. (2019). Third generation of vortex identification methods: Omega and Liutex/Rortex based systems. Journal of Hydrodynamics, 31(2), 205-223.

Liu, C., Gao, Y., Tian, S., & Dong, X. (2018). Rortex—A new vortex vector definition and vorticity tensor and vector decompositions. Physics of Fluids, 30(3), 035103.

Morino L. (1986). "Helmholtz decomposition revisited: vorticity generation and trailing edge condition," *Computational Mechanics*, 1(1): 65-90.

Wang, J., Zhao, W., and Wan, D. C. (2019). "Development of naoe-FOAM-SJTU solver based on OpenFOAM for marine hydrodynamics," *Journal of Hydrodynamics*, 31(1), 1–20.

Zhuang, Y., Wan, D.C., Benjamin, B., Ferrant, P. (2018) "Regular and Irregular Wave Generation in OpenFOAM using High Order Spectral Method," *The 13th OpenFOAM Workshop (OFW13)*, June 24-29, Shanghai, China, pp.189-192.

Zhuang, Y., Wan, D.C., Benjamin, B., Ferrant, P. (2020) "A Combined Method of HOS and CFD for Simulating a Container Ship in Steep Waves, " *The 33rd Symposium on Naval Hydrodynamics*.

Zhuang, Y., Wan, D.C., Li, Z., H. (2020) "Freak Wave-Induced Ship Motion with Sloshing Tanks Based on a HOS-CFD Coupling Method," *Proceeding the Thirtieth (2020) International Ocean and Polar Engineering Conference*, Shanghai, China, October 11-16, pp.2465-2471

Zhuang, Y., Wan, D.C. (2021) "Parametric study of a new HOS-CFD coupling method," *Journal of Hydrodynamics*, 33(1): 43-54.